ROYAL SOCIETY
OF CHEMISTRY

Check for updates

Exploring the changes in anticoagulant active ingredients before and after bovine bile fermentation of the traditional Chinese medicine Yaomu *via* an aggregation-induced emission fluorescence sensor

Qian Qin,†[abc] Jinwei Zhang,†[d] Guo Feng,*[ae] Yinhao Liao,[f] Youli Chen,[f] Caiyao Han,[a] Yan Lei,[a] Kexin Ma,[a] Wei Li,[ae] Yibao Jin,[b] Jinxi Wang,[c] Ping Wang,[b] Bing Wang*[b] and Xie-an Yu*[b]

Fermentation is a significant and specialized processing technology that primarily serves to enhance efficacy and reduce toxicity. Yaomu (YM) was fermented in a cellar using bovine bile as the fermentation matrix. However, the alterations in its active ingredients before and after processing remain poorly understood. An aggregation-induced emission fluorescence sensor (NITPA-S) was developed that employed S-2238 (S) to encapsulate the NITPA-Py-603 (NITPA) probe with the help of glutaraldehyde, creating an "ON" state. Thrombin hydrolyzed the sensor, releasing the probe in the "OFF" state, while thrombin inhibitors reversed this effect. We combined an HPLC fully automatic partial fraction collector and UHPLC-Q-TOF/MS for the separation, screening and identification of YM active compounds, which were used as indicators of anticoagulant activity to explore the changes in the content of YM before and after processing by using UHPLC-MS/MS and the sensor. A total of 211 compounds were collected and identified. Notably, karakoline, talatisamine, neoline, chasmanine and schaftoside exhibited the highest inhibition rates in YM. Furthermore, these compounds generally increased in concentration after processing ($p < 0.05$). The anticoagulant inhibition rates of the mixture of these five compounds were 86.48% and 83.44% when compared with those of unfermented YM and YM, respectively. Consequently, the fluorescent sensor could completely screen out the anticoagulant active ingredients, providing a novel analytical approach for exploring and screening changes in the active components before and after TCM processing.

1. Introduction

Processing plays a crucial role in traditional Chinese medicine (TCM).[1,2] The primary purpose of this process is to purify, pulverize, and remove odors from medicinal materials, thereby facilitating their preparation.[3] Notably, certain TCM substances are toxic, and only proper processing can ensure both safety and efficacy in clinical use.[4–9]

Yaomu (YM) is an important traditional medicine from Guizhou Province, which undergoes a specialized fermentation process.[10] YM is produced by fermenting a mixture of Arisaema Rhizoma, Pinelliae Rhizoma, Typhonii Rhizoma, Aconiti Radix, Curcumae Radix, Liushenqu, and bovine bile under controlled temperature, humidity, and moisture conditions. Fermentation is a crucial and special processing technique that employs microbes to reduce toxicity, enhance efficacy, and improve the original properties or generate new effects of traditional Chinese medicine (TCM).[11,12] Currently, YM is primarily used in combination with other drugs to treat ischemic stroke.[13] Through metabolomics and network pharmacology, our research group has demonstrated that processed YM enhances the treatment of ischemic stroke.[14] Therefore, it has been established that YM possesses anticoagulant effects. However, the pharmacologically active ingredients responsible for its anticoagulant properties remain unidentified, and the changes

[a]Department of Chinese Materia Medica, Guizhou University of Traditional Chinese Medicine, Guiyang 550025, China. E-mail: 453989352@qq.com

[b]NMPA Center for Innovation and Research in Regulatory Science, Shenzhen Institute for Drug Control, Shenzhen, 518057, China. E-mail: wangbingszyj@163.com; yuxieanalj@126.com

[c]Qiandongnan Miao and Dong Autonomous Prefecture Institute of Ethnic Medicine, Kaili City, Guizhou Province, 556000, China

[d]Chongqing University, Chongqing 400044, China

[e]Guizhou Inheritance Base of Traditional Chinese Medicine Processing Technology, Guizhou, China

[f]Zunyi Liaoyuan Hetang Pharmaceutical Co., Ltd, Zunyi, Guizhou 563005, China

† These authors contributed equally.

occurring before and after the fermentation of bovine bile have not been thoroughly reported. Thus, studying the alterations in anticoagulant active ingredients before and after YM fermentation is of great significance.

Currently, the methods employed for detecting changes in active ingredients include chromatography,[15] spectroscopy,[16] mass spectrometry,[17] electrophoresis,[18] electrochemical methods,[19] and instrument combination.[20] On the other hand, the techniques used for screening thrombin inhibitors encompass an online immobilized enzyme microreactor,[21] molecular docking,[22] database screening,[23] magnetic nanoparticles immobilization,[24] spectrum-effect relationship,[25] microfluidic technology,[26] affinity ultrafiltration,[27] and thrombin magnetic bead immobilization.[28] However, in practical applications, these methods not only fail to facilitate the rapid screening and analysis of active ingredients but are also costly, require a high level of expertise, and necessitate large sample sizes. Consequently, there is an urgent need to establish a rapid, economical, convenient method that requires a smaller sample size for screening and monitoring the active components before and after the processing of TCM.

Fluorescence sensors are analytical tools based on molecular recognition. They primarily utilize the interaction between the recognition group and the target analyte to induce changes in the fluorescence signal, thereby facilitating the qualitative and quantitative analysis of the target analyte.[29] Fluorescence sensors enable high-selectivity detection and multiplex screening of specific analytes, including proteins,[30,31] small organic molecules[32,33] and ions.[34,35] Through molecular design, they have excellent tunability, making them suitable for multiplex detection and real-time monitoring.[36,37] Currently, there are no reports on the application of sensors in monitoring the changes in active compound components before and after the fermentation of TCM. Therefore, we aim to prove that sensor technology can be employed to screen anticoagulant active ingredients before and after the fermentation of YM with bovine bile.

In this study, we have designed and synthesized a novel aggregation-induced emission (AIE) fluorescence sensor for exploring the anticoagulant active ingredients before and after bovine bile fermentation of YM. NITPA-Py-603 (NITPA) and S-2238 (S) were dissolved in a 10% tetrahydrofuran (THF)–H_2O solution and subsequently cross-linked with glutaraldehyde to construct the NITPA-S sensor, which exhibited stable fluorescence in the "ON" state (Scheme 1A). In the presence of thrombin, the substrate undergoes hydrolysis, releasing NITPA and resulting in the "OFF" state. Furthermore, when a thrombin inhibitor is present, thrombin activity is inhibited, causing the sensor's fluorescence to return to the "ON" state. Thus, the fluorescence change from "OFF" to "ON" can be utilized for screening thrombin inhibitors in YM (Scheme 1B). An HPLC-fully automatic partial fraction collector (HPLC-FC) and UHPLC-Q-TOF/MS were employed to further separate and identify YM. The sensor was then used to further screen the best anticoagulant components, which were used as anticoagulant activity indicators to explore the changes in the anticoagulant active ingredients before and after YM fermentation with bovine
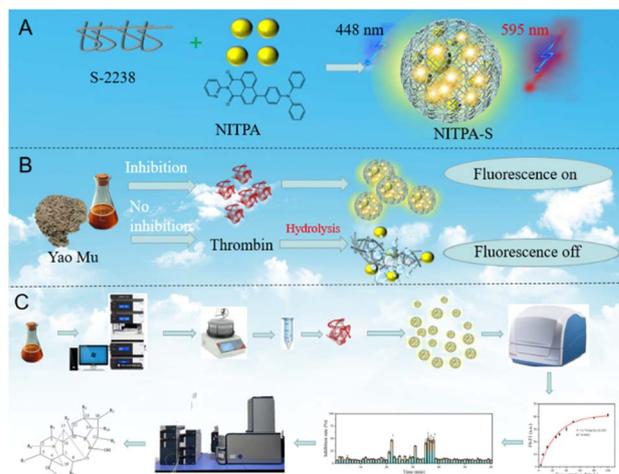
Scheme 1 The overall workflow chart of this study. (A) Schematic for the construction of the NITPA-S fluorescence sensor. (B) Schematic diagram of the screening of thrombin inhibitors by NITPA-S. (C) The flow chart for the screening of thrombin inhibitors from YM.

bile, and the results were subsequently validated by UHPLC-MS/MS (Scheme 1C). A total of 211 compounds were collected and identified. Notably, karakoline, talatisamine, neoline, chasmanine and schaftoside exhibited the highest inhibition rates. The concentrations of these compounds generally increased after processing ($p < 0.05$). The anticoagulant inhibition rate was further verified by the sensor to be 86.48% and 83.44% before and after bovine bile fermentation of YM, respectively. Therefore, this sensor can be used to explore the changes in the active ingredients before and after YM fermentation. This study has provided a novel analytical method for exploring and screening changes in the active ingredients in TCM before and after processing.

2. Materials and methods

2.1 Materials

Yaomu and unfermented Yaomu were supplied by Zunyi Liaoyuan Hetang Pharmaceutical Co., Ltd (Guizhou, China). NITPA was procured from Xi'an Ruixi Biological Technology Co., Ltd (Shaanxi, China). Tetrahydrofuran, argatroban, formic acid (chromatographic grade), α-glucosidase, creatine kinase, superoxide dismutase, lactate dehydrogenase and glutaraldehyde were supplied by Aladdin Biochemical Technology Co., Ltd (Shanghai, China). Thrombin and albumin were sourced from Macklin Biochemical Co., Ltd (Shanghai, China). S-2238 was obtained from Asrel Biotechnology Co., Ltd (Beijing, China). Acetonitrile and methanol (both chromatographic grade) were obtained from Merck Co., Ltd (Germany). Karakoline, talatisamine, neoline, chasmanine, schaftoside and lappaconitine were provided by Xili Biotechnology Co., Ltd (Yunnan, China). Rutin was acquired from Yuanye Biotechnology Co., Ltd (Shanghai, China). Phosphate-buffered saline (PBS) (1 M, pH 7.2–7.4) was obtained from Boster Biological Technology Co., Ltd (Wuhan, China). Tris-buffered saline (1 M, pH 7.4) was

purchased from Solarbio (Beijing, China). Experimental water was purified using a Millipore water purification system.

2.2 Instruments

Fluorescence detection was conducted using a microplate reader (Thermo Scientific Varioskan Flash, Switzerland). UV-vis absorbance was performed with a UV-2450 spectrophotometer (Shimadzu Company, Japan). Additionally, dynamic light scattering (DLS) and zeta potential characterization were carried out using a Zetasizer Nano-Z instrument (Malvern, UK). HPLC was executed utilizing an UltiMate 3000 system (Thermo Fisher Scientific, USA). UHPLC-Q-TOF/MS analyses were performed on an AB SCIEX X500R mass spectrometer (AB SCIEX, USA), equipped with SCIEX-OS software. The quantification of YM was performed using a SCIEX Triple Quad 4500 MS System (AB SCIEX, USA).

2.3 Synthesis and characterization of the NITPA-S sensor

The synthesis of the NITPA-S sensor proceeded as follows: a total reaction volume of 2.0 mL was prepared in a brown vial. Initially, NITPA (50 μM) was dissolved in a 90% H_2O–THF solution. Subsequently, S-2238 (0.5 mg mL^{-1}) and the cross-linker glutaraldehyde (0.75%, v/v) were added and mixed at 200 rpm for 30 minutes in the dark. The reaction system was then uncovered for 12 hours to evaporate excess tetrahydrofuran. The prepared NITPA-S sensor was then stored in a 4 °C refrigerator away from light. The synthesized fluorescence sensor was utilized to determine the excitation and emission wavelengths using a microplate reader. The UV-vis absorption, zeta potential, and DLS of NITPA, S-2238, and the sensor were measured at room temperature.

2.4 Detection of thrombin by the NITPA-S sensor

Thrombin was detected by using the above optimized incubation conditions. The specific steps were as follows: 10 μL of thrombin at varying concentrations was added to 40 μL of PBS buffer in a black 96-well plate. The solution was mixed for 1 minute and incubated for 5 minutes at 37 °C. Subsequently, 10 μL of Milli-Q water was added to the well, mixed for 1 minute, and incubated at 37 °C for an additional 10 minutes. Following this, 40 μL of the NITPA-S sensor was added, mixed again for 1 minute, and incubated for 20 minutes at 37 °C. In the screening of thrombin inhibitors, 10 μL of Milli-Q water was substituted with 10 μL of YM extract, and the remaining steps were performed as previously described. Concurrently, the specificity of the sensor for thrombin was verified under the same conditions by replacing thrombin with an equivalent concentration of other proteases, including α-glucosidase, albumin, creatine kinase, superoxide dismutase, and lactate dehydrogenase. Finally, the fluorescence spectra of the mixture were collected using an excitation wavelength of 448 nm, and fluorescence intensities were measured at 448 nm (excitation) and 595 nm (emission).

2.5 Screening of anticoagulant active compounds from YM

To obtain the YM solution, YM was extracted by adding 70% methanol and subjecting it to ultrasonication for 30 minutes, followed by centrifugation at 14 000 rpm for 10 minutes. Subsequently, the HPLC method was developed by optimizing the mobile phase, column temperature, flow rate, and wavelength, resulting in the collection of 60 fractions at one-minute intervals using HPLC-FC. The collected fractions were dried under nitrogen and reconstituted with 100 μL of 70% methanol to yield sample fractions, which were screened for anticoagulant activity according to the method described in Section 2.4 to isolate the anticoagulant components. Finally, the UHPLC method was established by further optimizing the mobile phase, column temperature, flow rate, and other conditions. The IDA full scan mode was selected for Q-TOF/MS, and UHPLC-Q-TOF/MS was utilized to identify the fractions of the YM solution and the anticoagulant compounds.

2.6 Exploring the changes in anticoagulant active compounds before and after the fermentation of YM

The optimal anticoagulant components were selected as indicators to investigate the changes before and after YM fermentation using UHPLC-MS/MS. Initially, the UHPLC fingerprint was established by optimizing the mobile phase conditions, column temperature and flow rate. The mass spectrometric intensities for the five compounds and two internal standards (ISs) were optimized by infusing standard solutions of each compound into the mass spectrometer, adjusting parameters such as declustering potential (DP) and collision energy (CE) to enhance the sensitivity of the multiple reaction monitoring (MRM) mode. Lappaconitine (IS1) served as the internal standard for karakoline, talatisamine, neoline, and chasmanine, while rutin (IS2) was utilized as the internal standard for schaftoside. Subsequently, the five compounds were assessed for linearity, accuracy, stability, recovery, and reproducibility to evaluate YM before and after processing using UHPLC-MS/MS. Finally, based on the concentration of each compound in the YM solution, a mixed standard solution was prepared and diluted to match the concentration of the YM solution, enabling the assessment of their thrombin inhibition rates using the sensor.

3. Results and discussion

3.1 The characteristics of NITPA

The restricted intramolecular motion (RIM) and intramolecular charge transfer (ICT) mechanisms of NITPA molecules enable the sensor to exhibit intense fluorescence. In the NITPA molecule, the triphenylamine unit serves as the molecular rotor. In the dispersed state, its free rotation provides an efficient non-radiative decay channel for the excited state energy, leading to fluorescence quenching. When molecules aggregate to form a closed environment, the rotation of triphenylamine is restricted, which effectively blocks the non-radiative decay channel, causing excited-state electrons to mainly return to the ground state through radiative transitions, thereby generating
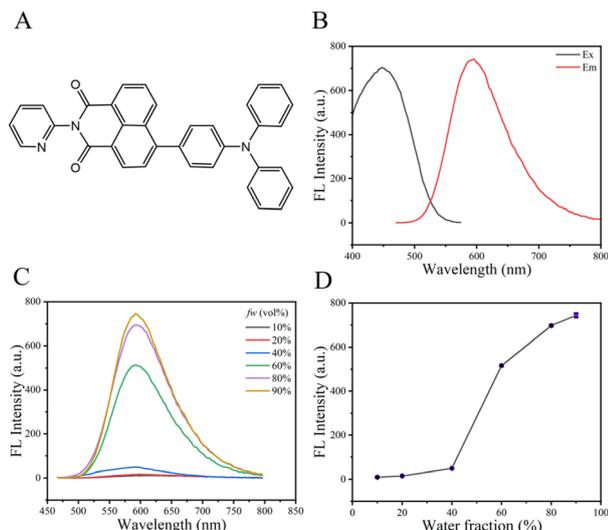
Fig. 1 The characteristics of NITPA (λ_{ex} = 448 nm, λ_{em} = 595 nm, n = 3). (A) Structure of NITPA. (B) The fluorescence excitation and emission spectra of NITPA in 90% H_2O−THF. (C) Fluorescence spectra and (D) the intensity of NITPA in the 10% to 90% H_2O−THF mixture solutions (λ_{ex} = 448 nm, λ_{em} = 595 nm, and n = 3).

Fig. 2 Synthesis conditions of the sensor. The fluorescence emission spectra and intensity of the sensor with different (A and B) concentrations of S-2238 and (C and D) volumes of glutaraldehyde (λ_{ex} = 448 nm, λ_{em} = 595 nm, and n = 3).

significant fluorescence and demonstrating the AIE effect. Additionally, NITPA fluorescence is enhanced due to the attachment of a benzene ring at the 4-position of the naphthalimide, with a substituent also linked to this benzene ring, forming the characteristic donor–π–acceptor (D-pi–A) structure[38] (Fig. 1A). Furthermore, in a 90% H_2O–tetrahydrofuran (THF) solution, the maximum excitation and emission wavelengths of NIPTPA were measured to be 448 nm and 595 nm (Fig. 1B) by using an enzyme labeler. Meanwhile, the UV-visible wavelength of NITPA was determined to be 448 nm (Fig. S1). Additionally, in verifying NITPA aggregation-induced luminescence, the results revealed that fluorescence intensity increased progressively when NITPA was dispersed in 10% to 90% H_2O–THF solution (Fig. 1C) and NITPA had optimal fluorescence intensity in 90% H_2O–THF (Fig. 1D). Therefore, we analyzed the above to demonstrate that the NITPA probe had an aggregation-induced luminescence effect, and 90% H_2O–THF was chosen as the optimal ratio for subsequent sensor synthesis.

3.2 Synthesis and characterization of the NITPA-S sensor

The synthesis of the NITPA-S sensor utilized a single-variable control method to optimize substrate concentration, glutaraldehyde volume, magnetic stirrer speed, and reaction time in order to achieve the most favorable synthesis conditions. As illustrated in Fig. 2A, the fluorescence intensity of the NITPA-S sensor initially increased and subsequently decreased with an increase in substrate concentration from 0.25 mg mL^{-1} to 1.25 mg mL^{-1}, with 0.5 mg mL^{-1} determined to be the optimal concentration (Fig. 2B). A comparable trend was noted when optimizing the glutaraldehyde volume (Fig. 2C), with the highest fluorescence intensity attained at a glutaraldehyde volume ratio of 0.75% (v/v) (Fig. 2D). Moreover, the stirring speed and reaction time of the magnetic stirrer were optimized, revealing
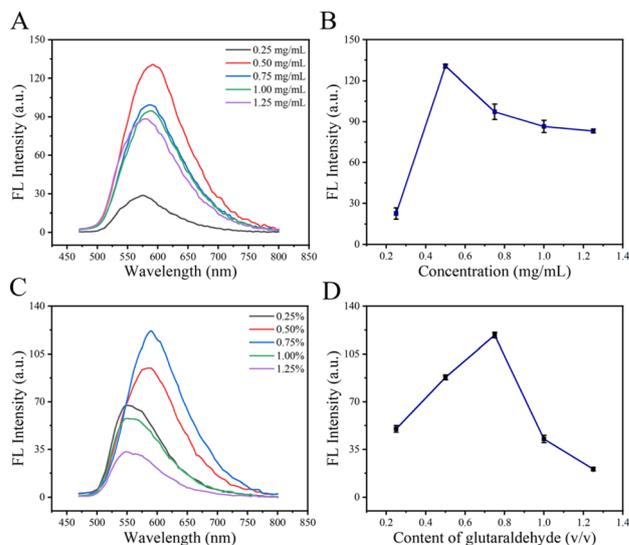
that a stirring speed of 200 rpm (Fig. S2A and B) for a duration of 0.5 hours (Fig. S2C and D) yielded maximum fluorescence intensity, which was selected as the optimal synthesis condition. In summary, the synthesis steps for the sensor were as follows: 50 μM of the probe was added to a 90% H_2O–THF solution, followed by the addition of 0.5 mg mL^{-1} of substrate and 0.75% (v/v) glutaraldehyde. This mixture was then stirred in a magnetic stirrer at 200 rpm in the dark for 30 minutes.

The optimal excitation and emission wavelengths of the NITPA-S sensor were 448 nm and 595 nm, respectively (Fig. 3A). In addition, UV-vis spectroscopy revealed characteristic
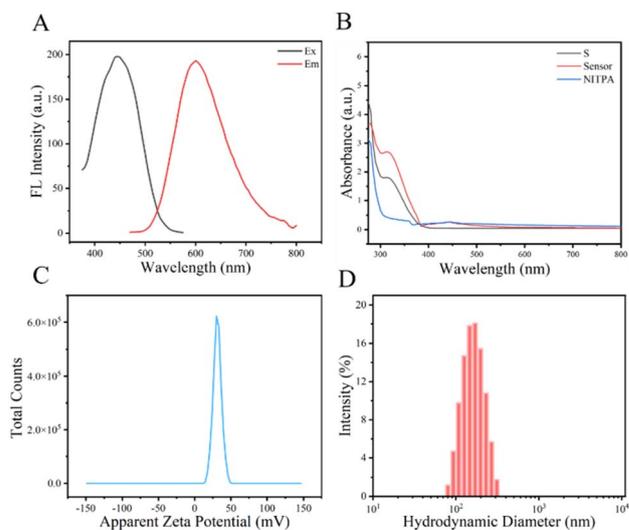

Fig. 3 The characterization of the sensor. (A) Fluorescence excitation and emission spectra, (B) UV-vis absorption spectra, (C) zeta potential and (D) hydrodynamic size of the sensor (λ_{ex} = 448 nm, λ_{em} = 595 nm, and n = 3).

absorption peaks at 320 nm and 448 nm (Fig. 3B). The approximate zeta potential of the sensor was measured to be +40 mV (Fig. 3C), while S-2238 exhibited a zeta potential of 5 mV (Fig. S3A) and that of NITPA was −30 mV (Fig. S3B). Charge transfer was observed following the encapsulation of NITPA by S-2238, confirming the successful encapsulation of NITPA. Additionally, DLS analysis indicated that the average hydrodynamic diameter of the sensor was 197 nm (Fig. 3D), with S-2238 and NITPA measuring 100 nm (Fig. S4A) and 125 nm (Fig. S4B), respectively. DLS results demonstrated a gradual increase in the average hydrodynamic diameter of the sensor, supporting the conclusion that successful combination occurred. Subsequent measurements of hydrated particle size (Fig. S5A), zeta potential (Fig. S5B), and fluorescence intensity (Fig. S5C) over a consecutive week revealed minimal changes, indicating good stability. Therefore, the experimental data for synthesis optimization, characterization and stability fully proved the successful construction of the sensor.

3.3 Detection of thrombin based on the NITPA-S sensor

Under the influence of the glutaraldehyde crosslinking agent, the NITPA fluorescent probe was encapsulated by the S-2238 substrate molecule, leading to the aggregation of the probe molecules. At this stage, the NITPA-S sensor system exhibited a fluorescence "ON" state. Upon the addition of thrombin, the enzyme specifically cleaved the S-2238 substrate, thereby releasing the encapsulated NITPA probe and resulting in the "OFF" state of the fluorescence signal of the sensor system. To optimize the reaction between thrombin and the substrate, we systematically adjusted the reaction conditions using a univariate control method. The type and concentration of the buffer were analyzed, as shown in Fig. S6A, indicating that the hydrolysis sensor was more effectively hydrolyzed by thrombin in 10 mM PBS. This finding confirmed that thrombin activity was optimal in a 10 mM PBS buffer. Additionally, we investigated the effects of reaction temperature and time. Thrombin activity increased between 25 °C and 37 °C but decreased when the temperature exceeded 37 °C, likely due to enzyme inactivation (Fig. S6B). The fluorescence intensity did not continue to decrease after incubation at 37 °C for 20 minutes (Fig. S6C). Therefore, based on the data presented, thrombin was added to the 10 mM PBS buffer solution and incubated at 37 °C for 20 minutes after the addition of 50 μL of the fluorescence sensor, establishing the optimal incubation conditions for the subsequent preparation of the standard curve.

In order to reflect the relationship between different thrombin concentrations and the change in fluorescence intensity, after adding different concentrations of thrombin, a curve was made with the intensity of fluorescence change as the ordinate and the concentration of thrombin as the abscissa. The curve $Y = 11.721 \ln(X) - 12.529$ had a linear range of 3.125 U mL^{-1} to 100.0 U mL^{-1} with a correlation of $R^2 = 0.9901$, as shown in Fig. 4A (F_0 represents the fluorescence intensity before the sensor reaction; F_1 is the fluorescence intensity after the thrombin reaction), which showed a good linear relationship between the fluorescence intensity and concentration of
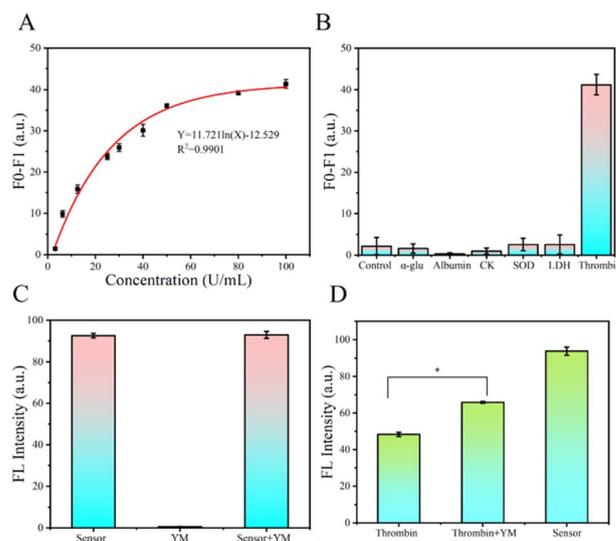

Fig. 4 The response of the sensor to thrombin (λ_{ex} = 448 nm and λ_{em} = 595 nm). (A) Polynomial regression curve and linear regression curve with thrombin concentrations ranging from 3.125 U mL^{-1} to 100 U mL^{-1}. (B) Specificity analysis of the sensor in the presence of different proteases. (C) The fluorescence intensities of the sensor, YM, and YM + sensor. (D) The fluorescence intensity of thrombin + sensor, thrombin + sensor + YM and sensor (n = 3 and *p < 0.05).

thrombin. Another function of this curve was that in the screening of thrombin inhibitors, the concentration of thrombin was determined by the difference in fluorescence in the reaction between the compound and thrombin, which could be used to calculate the thrombin inhibition rate. When the concentration of thrombin exceeded 50 U mL^{-1}, the fluorescence intensity changed slightly. Thus, 50 U mL^{-1} was selected as the thrombin concentration for anticoagulant screening in subsequent experiments.

The sensor specificity experiment demonstrated that the sensor exhibited high specificity, reacting exclusively with thrombin and showing no response to α-glucosidase (α-Glu), albumin, creatine kinase (CK), superoxide dismutase (SOD), or lactate dehydrogenase (LDH) (Fig. 4B). Next, it was explored whether the YM extract responded to the sensor. The results showed that the YM extract did not affect the fluorescence intensity of the NITPA-S sensor (Fig. 4C). Subsequently, the anticoagulant effect of the YM extract was verified. The experimental data showed that the addition of YM extract to the system increased the fluorescence intensity compared to the addition of thrombin alone (Fig. 4D), which indicated that YM can inhibit thrombin and be used to screen inhibitors. Finally, the positive control drug argatroban was also tested, and the IC$_{50}$ measured by the NITPA-S sensor was 2.691 μM (Fig. S7), which was similar to the previously published data.[39] Therefore, the above experimental data further proved that the NITPA-S sensor could be used to screen thrombin inhibitors from YM.

3.4 Screening anti-thrombin activity from YM extract

Firstly, the HPLC analysis method of YM extract was established by optimizing various chromatographic conditions. To achieve

optimal peak separation and baseline stability, acetonitrile (A) and 0.1% formic acid in water (B) were selected as the mobile phase. The flow rate was maintained at 1.0 mL min^{-1} using a Waters XBridge C18 column (250 mm × 4.6 mm, 5 μm) at a temperature of 40 °C. The elution gradient is detailed in Table S1. Subsequently, 60 fractions were collected at 1-minute intervals and dried under nitrogen. These fractions were then re-dissolved in 70% methanol and tested for thrombin inhibitory activity using the sensor, as no inhibitory effect of 70% methanol on the sensor reaction system was observed (Fig. S8). Measurement of the anticoagulant activity of each fraction revealed that the active components were primarily concentrated between 23 and 39 minutes (Fig. 5A).

UHPLC-Q-TOF/MS was employed to analyze the YM extract and its thrombin-inhibiting components. The final UHPLC method utilized a mobile phase consisting of 0.1% formic acid aqueous solution (A) and acetonitrile (B) with a flow rate of 0.3 mL min^{-1}. The chromatographic analysis was performed using a Waters ACQUITY UPLC HSS T3 column (150 mm × 2.1 mm, 1.8 μm) at a temperature of 40 °C, with the elution gradient detailed in Table S2. By referencing chemical databases and relevant literature, including PubChem, and by correlating with retention times, a total of 211 compounds in the YM extract were structurally identified using SCIEX OS data processing software, which included 101 alkaloids (13 diesters, 32 monoesters, 47 alcohol amines, and 9 other alkaloids), 32 sesquiterpenes, 22 bile acids, 9 amino acids, 7 nucleosides, 8 lysophosphatidylcholines, 7 amides, 7 alcohol ethers, 7 fatty acid glycerides, and 11 other compounds (Table S3). In the meantime, fractions 23, 35, 36, 37, and 38 were identified as karacoline, neoline, chasmanine, schaftoside, and talatisamine, respectively (Fig. 5B). Consequently, we used the constructed

sensor to screen the compounds of anticoagulant components in YM, these 5 compounds were screened and used as indicators of anticoagulant components for the subsequent study of active components before and after fermentation of YM.

3.5 Verification and exploration of the changes in the anticoagulant activity of YM and unfermented YM extract

On the one hand, the mass spectrometry (MS) parameters, including the declustering potential (DP) and collision energy (CE), were optimized to enhance the sensitivity of the multiple reaction monitoring (MRM) method (Table S4). On the other hand, the mobile phase consisted of 0.1% formic acid in water (component A) and acetonitrile (component B), with a flow rate of 0.3 mL min^{-1}. The chromatographic analysis employed a Waters Acquity UPLC HSS T3 column (150 × 2.1 mm, 1.8 μm), maintained at a temperature of 40 °C with the elution gradient detailed in Table S5. Consequently, the subsequent experiments integrated the MRM channel with the UHPLC method to develop the methodology and quantify the analyte content.

The subsequent phase in the advancement of quantitative methodologies is outlined as follows. Initially, the compound peaks were obtained, and no interference was detected between the tested compounds and the internal standards, as illustrated in Fig. S9. The linear regression equations, correlation coefficients, linear response ranges, detection limits, and quantitation limits for the five components are detailed in Table S6, indicating that the correlation coefficients (R) for the five compounds varied between 0.9938 and 0.9991. Utilizing a signal-to-noise ratio (S/N) greater than 5 as the lower limit of quantification (LLOQ), the LLOQ for the four alkaloids was determined to be 0.05 ng mL^{-1}, while that for schaftoside was 5 ng mL^{-1}. Subsequently, intraday precision, interday precision, and stability were assessed at three concentration levels. The results showed that the relative standard deviation (RSD) values for intraday and interday precision ranged from 1.23% to 5.05% and 1.17% to 8.84%, respectively, with accuracy values falling between 86.22% and 109.8%. The RSD for stability was found to range from 2.23% to 7.35%, and the accuracy was between 87.15% and 110.7% (Table S7). The repeatability of the method was validated using six parallel samples from the same batch. The RSD of the five compounds in the raw material ranged from 0.44% to 1.91% (Table S8), indicating good repeatability of the method. Additionally, quantitative accuracy was confirmed through recovery tests conducted at three concentrations (Table S9). The average recovery rates ranged from 95.30% to 105.5%, with an RSD of less than 9.44%, satisfying recovery requirements. Therefore, the data indicate that this method meets the standards for quantitative analysis of the five compounds in the raw material and effectively measures their contents before and after processing with YM. The contents of the five components in six batches of unfermented and fermented YM were determined, with results showing that the concentrations of bovine bile before and after fermentation are detailed in Fig. 6A and Table S10, which clearly demonstrate higher levels of these five compounds after fermentation ($p < 0.05$). Furthermore, at the same dilution, the inhibition rate of YM was higher post-
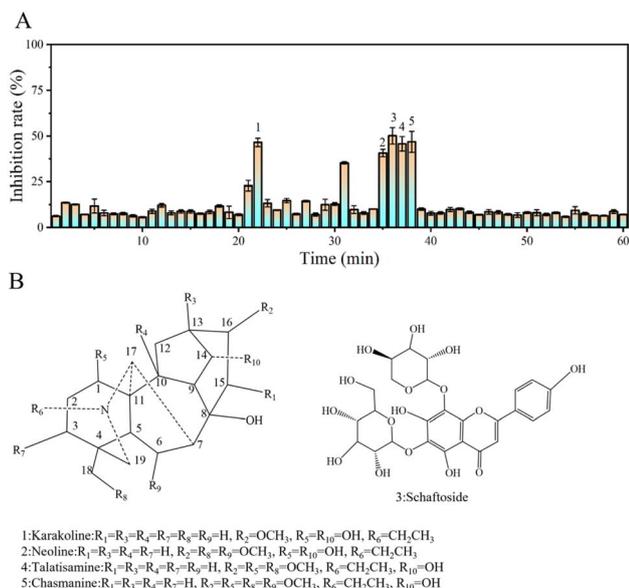

Fig. 5 The inhibitory rates and chemical structures of active components. (A) The inhibitory rates of YM extract fractions on thrombin. (B) The chemical structures of four alkaloids and schaftoside ($\lambda_{ex} = 448$ nm, $\lambda_{em} = 595$ nm, and $n = 3$).
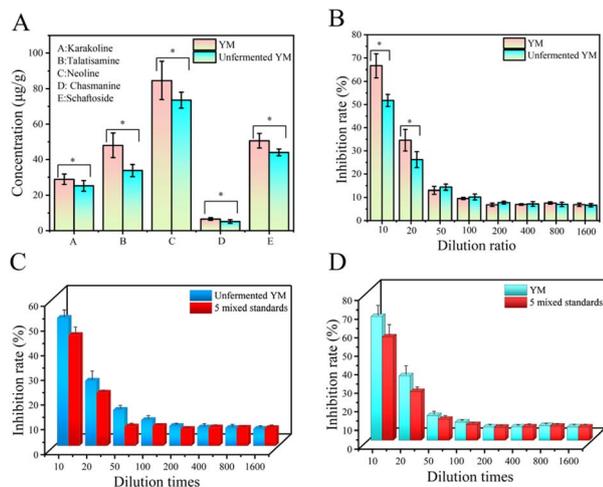
Fig. 6 Content determination and inhibition rate analysis of five compounds. (A) The contents of five compounds before and after YM processing. (B) The inhibitory activity of YM and unfermented YM. The inhibitory activity of (C) YM and (D) unfermented YM and mixed standard solutions of five compounds (karakoline, talatisamine, chasmanine, neoline and schaftoside, λ_{ex} = 448 nm, λ_{em} = 595 nm, n = 3, and $*p$ < 0.05).

fermentation compared to pre-fermentation (Fig. 6B, p < 0.05). Thus, the data indicate that YM exhibits changes in anticoagulant components before and after fermentation. The fluorescence sensor has been validated as an effective tool for exploring changes in active ingredients before and after processing TCM.

Additionally, we conducted a comparative analysis of thrombin inhibition rates for the five compounds and YM, both before and after fermentation. Based on the concentrations of the five compounds before and after processing of YM, corresponding mixed standard solutions were prepared, diluted in the same proportion as YM and unfermented YM, and evaluated for anticoagulant activity (Fig. 6C and D). The data revealed that the anticoagulant effects of the mixture of these five compounds before and after processing were 86.48% and 83.44%, which indicated that the anticoagulant components in this screening had anticoagulant effects representative of the raw material. In summary, this fluorescence sensor could screen anticoagulant components and explore changes in the active ingredients before and after bovine bile fermentation of YM.

4. Conclusions

In conclusion, the fluorescence sensor NITPA-S was successfully synthesized and is suitable for the screening of anticoagulant components. A total of 211 compounds were identified, including 13 diesters, 32 monoesters, 47 alcohol amines, 9 other alkaloids, 32 sesquiterpenes, 22 bile acids, 9 amino acids, 7 nucleosides, 8 lysophosphatidylcholines, 7 amides, 7 alcohol ethers, 7 fatty acids; 11 other compounds with karakoline, talatisamine, neoline, chasmanine, and schaftoside exhibited significant thrombin inhibition rates in YM. It was found that

the thrombin inhibition rates of five compounds were equivalent to 86.48% and 83.44% when compared with unfermented YM and YM, respectively. Bovine bile fermentation increased the levels of these five compounds in YM, which enhanced the anticoagulant effect. Therefore, this study provides a new analytical method for exploring the changes in the active ingredients and the material basis before and after processing of TCM.

Author contributions

Qian Qin: conceptualization, data curation, formal analysis, writing – original draft and methodology. Jinwei Zhang: conceptualization, data curation, formal analysis, writing – original draft, methodology. Guo Feng: data curation, funding acquisition, project administration, resources, writing – review and editing. Yinhao Liao and Youli Chen: project administration. Caiyao Han: software, methodology. Yan Lei: validation. Kexin Ma: investigation. Wei Li: resources, validation. Yibao Jin: formal analysis. Jinxi Wang and Ping Wang: data curation. Bing Wang: data curation, funding acquisition, project administration, resources, writing – review and editing. Xie-an Yu: data curation, funding acquisition, project administration, resources, writing – review and editing.

Conflicts of interest

The authors declare no competing interests.

Data availability

Data are included within the article and supplementary information (SI). Supplementary information is available. See DOI: https://doi.org/10.1039/d5ra09117a.

Acknowledgements

References

1 Z. Chen, S. Y. Ye and R. G. Zhu, *Pharm. Biol.*, 2020, **58**, 561–573.

2 X. Wu, S. Wang, J. Lu, Y. Jing, M. Li, J. Cao, B. Bian and C. Hu, *Chin. Med.*, 2018, **13**, 4.

3 R. L. Li, Q. Zhang, J. Liu, L. Y. He, Q. W. Huang, W. Peng and C. J. Wu, *J. Integr. Med.*, 2021, **19**, 89–103.

4 S. Song, R. Qiu, X. Jin, Z. Zhou, J. Yan, Q. Ou, X. Liu, W. Li, Y. Mao, W. Yao and T. Lu, *J. Ethnopharmacol.*, 2022, **287**, 114911.

5 Y. Fan, Z. Li and J. Xi, *RSC Adv.*, 2020, **10**, 1410–1425.

6 X. Song, G. Feng, C. Ren, W. Li, W. Liu, G. Liu, J. Zhang, Y. Lei, Z. He, C. Han, T. Liu, K. Ma and J. Hou, *J. Ethnopharmacol.*, 2024, **324**, 117770.

7 E. Xu, M. Sang, W. Xu, Y. Chen, Z. Wang, Y. Zhang, W. Lu and P. Cao, *J. Ethnopharmacol.*, 2024, **337**, 118794.

8 L. Zhong, J. Sun, S. Li, Y. Qi, M. Luo, L. Dong and J. Chen, *J. Ethnopharmacol.*, 2024, **333**, 118475.

9 T. Wang, Y. Song, H. Xu, Y. Liu, H. He, M. Zhou, C. Jin, M. Yang, Z. Ai and D. Su, *J. Ethnopharmacol.*, 2022, **290**, 115112.

10 G. Cao, F. Ma, J. Xu and Y. Zhang, *Lett. Appl. Microbiol.*, 2020, **70**, 318–325.

11 L. Li, L. Wang, W. Fan, Y. Jiang, C. Zhang, J. Li, W. Peng and C. Wu, *Am. J. Chin. Med.*, 2020, **48**, 899–921.

12 X. Luo, M. Dong, J. Liu, N. Guo, J. Li, Y. Shi and Y. Yang, *Front. Pharmacol*, 2024, **15**, 1430238.

13 P. Yang, H. He, S. Xu, P. Liu and X. Bai, *J. Evidence-Based Complementary Altern. Med.*, 2020, **2020**, 8872593.

14 C. Han, F. Feng, Q. Qin, W. Li, Y. Chen, G. Liu, Y. Lei, T. Liu, K. Ma, J. Hou, Y. Huang, M. Lin and J. Jiang, *J. Ethnopharmacol.*, 2025, **343**, 119438.

15 L. Ciurlă, I.-M. Enache and A. Patraș, *Molecules*, 2025, **30**, 3071.

16 C. K. Mitchell, J. C. Dumke, C. A. Corbett, L. M. Jones and K. E. Ceniccola-Campos, *J. Forensic Sci.*, 2024, **69**, 2222–2229.

17 D. Chen, J. Chen, Y. Shen, X. Chen, H. Xia, Y. N. Liu and R. A. Xu, *Pharm. Biol.*, 2024, **62**, 874–881.

18 X. Li, D. Wen, Y. He, Y. Liu, F. Han, J. Su, S. Lai, M. Zhuang, F. Gao and Z. Li, *Foods*, 2024, **13**, 4141.

19 H. Chi, C. Yang and G. Liu, *Food Chem.*, 2024, **452**, 139548.

20 F. Saintmont, Y. Ladner, C. Perrin, S. Dutertre and C. Bich, *Talanta*, 2025, **296**, 128462.

21 W. Liu, R. Zhou, J. Wen, J. Li, K. Du, J. He, Y. Yao and Y. Chang, *Phytochem. Anal.*, 2025, **36**, 520–528.

22 X. Zhang, X. Zheng, C. Han and L. Wu, *Front. Chem.*, 2024, **12**, 1451574.

23 L. Buitrago, M. R. Menezes, C. Larson, J. Li, T. Kartika, P. Banerjee, F. Glickman and B. Coller, *Blood Adv.*, 2025, **9**, 1049–1068.

24 H. Guo, L. Guo, J. Yu, F. Zhao, W. Yang, J. Li, H. Chen and J. Qian, *J. Pharm. Biomed. Anal.*, 2024, **243**, 116110.

25 X. Wang, D. Y. Zhang, S. J. Yin, H. Jiang, M. Lu, F. Q. Yang and Y. J. Hu, *Molecules*, 2021, **26**, 7293.

26 X. N. Wang, Y. Song, W. Tang, P. Li and B. Li, *Biosens. Bioelectron.*, 2023, **237**, 115527.

27 Q. Huang, J. Tang, X. Chai, W. Ren, J. Wang, Q. Gan, J. Shi, M. Wang, S. Yang, J. Liu and L. Ma, *J. Chromatogr. B: Anal. Technol. Biomed. Life Sci.*, 2021, **1178**, 122822.

28 J. Cao, J. J. Xu, X. G. Liu, S. L. Wang and L. Q. Peng, *J. Chromatogr. A*, 2016, **1468**, 86–94.

29 D. Zeng, B. Wang, Y. Guo, Q. Wang, X. Tang, Z. Xiao, X. Yao, C. Huang, W. Guo, M. Li, P. Wang, Q. Feng, X. A. Yu and Y. Dai, *Biosens. Bioelectron.*, 2025, **271**, 116994.

30 L. Han, B. Wang, K. Sun, M. Sitara, M. Li, P. Wang, N. Chen, X. A. Yu and J. Tian, *Analyst*, 2024, **149**, 3585–3595.

31 K. Du, B. Wang, S. Chen, Y. Chen, S. Wang, C. Liang, Y. Shang, C. Wang, S. Hou, J. Li, X. Yu and Y. Chang, *Sens. Actuators, B*, 2022, **370**, 132447.

32 S. Chen, K. Chen, K. Du, S. Wang, C. Liang, Y. Shang, X. Xie, G. Tang, J. Li, B. Wang, X. A. Yu and Y. Chang, *ACS Sens.*, 2023, **8**, 1431–1439.

33 P. Zhao, Z. Song, Y. Li, X. Liu, Z. Jiang, Q. Zhu and J. H. Qu, *J. Pharm. Biomed. Anal.*, 2025, **254**, 116570.

34 H. Li, Y. Zhong, R. Huang and R. Zhao, *Molecules*, 2019, **24**, 4593.

35 H. Wan, Q. Xu, P. Gu, H. Li, D. Chen, N. Li, J. He and J. Lu, *J. Hazard. Mater.*, 2021, **403**, 123656.

36 A. H. Upadhaya, H. A. Mirgane, S. P. Pandey, V. S. Patil, S. V. Bhosale and P. K. Singh, *Langmuir*, 2024, **40**, 19357–19369.

37 X. Zhai, Y. Kou, L. Liang, P. Liang, P. Su and Y. Tang, *Inorg. Chem.*, 2023, **62**, 18533–18542.

38 Y. Qu, L. Wang, J. Wu, Y. Rui, J. Cao and J. Xu, *Dyes Pigm.*, 2018, **148**, 99–107.

39 W. Liu, R. Zhou, J. Wen, J. Li, K. Du, J. He, Y. Yao and Y. Chang, *Phytochem. Anal.*, 2025, **36**, 520–528.